

Controlling the Spin-orbit Branching Fraction in Molecular Collisions

Cornelia G. Heid,[†] Imogen P. Bentham,[†] Victoria Walpole,^{†,§} Pablo G. Jambrina,[‡]
F. Javier Aoiz,[¶] and Mark Brouard^{*,†}

[†]*Department of Chemistry, University of Oxford, The Chemistry Research Laboratory, 12
Mansfield Road, Oxford, OX1 3TA, United Kingdom*

[‡]*Departamento de Química Física, Universidad de Salamanca, 37008, Salamanca, Spain*

[¶]*Departamento de Química Física, Facultad de Química, Universidad Complutense, 28040
Madrid, Spain*

[§]*Current address: Max Planck Institute for Biophysical Chemistry, Am Faßberg 11, 37077
Göttingen, Germany*

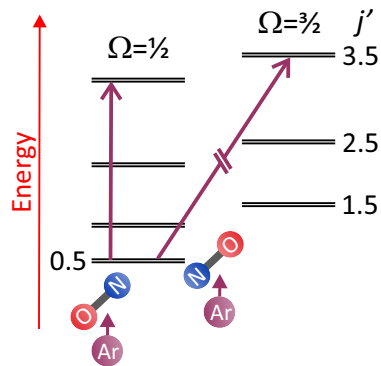
E-mail: mark.brouard@chem.ox.ac.uk.

November 9, 2020

Abstract

The collision geometry, that is, the relative orientation of reactants before interaction, can have a large effect on how a collision or reaction proceeds. Certain geometries may prevent access to a given product channel, while others might enhance it. In this letter, we demonstrate how the initial orientation of NO molecules relative to approaching Ar atoms determines the branching between the spin-orbit changing and the spin-orbit conserving rotational product channels. We use a recently developed quantum treatment to calculate differential and integral branching fractions - at any arbitrary orientation - from theoretical and experimental data points. Our results show that a substantial degree of control over the final spin-orbit state of the scattering products can be achieved by tuning the initial collision geometry.

TOC Graphic



In many inelastic or reactive molecular encounters, the spatial arrangement in which the collision partners approach each other plays a vital role in determining the outcome of the interaction. While a relative geometry that aligns with the reaction coordinate will facilitate product formation,^{1,2} a geometry in which access of the reaction coordinate is hindered will less efficiently lead to products.^{3,4} The trajectory a molecule or atom approaching from a specific direction will follow is governed by the attractive and repulsive forces that make up the local energy landscape. Control over the initial orientation thus also provides control over the reaction or collision pathway.⁵⁻⁸ In addition, there might be competing pathways associated with different product channels, and altering the initial spatial configuration may favor one channel over another.⁹

Molecules can be aligned with polarized laser light^{1,7,9-11} or oriented in an electric^{6,12-15} or magnetic¹⁶⁻¹⁸ field; these techniques make it possible to define parallel or perpendicular (alignment)^{1,7,9,10} and “end-on” or “side-on” collision geometries (orientation).^{6,12-15,19} Previous work on oriented NO + rare gas collisions has focused on end-on collisions, in which the rare gas atom approaches the NO either from the N-end or the O-end.^{15,20-22} More recently, we have investigated side-on collisions, in which we distinguished between (predominantly) repulsive collisions towards the N-side or towards the O-side of the NO molecule.^{19,23,24} However, in principle, our experimental setup allows for orientation of the NO molecules (as defined by a broad cosine distribution¹⁵) at any arbitrary angle relative to the collision partner.

Here, we investigate the implications of having full control over the range of possible collision geometries in terms of the spin-orbit branching fractions in the scattering of NO molecules with Ar atoms. We show how our recently developed quantum mechanical (QM) treatment of the scattering dynamics for electric field oriented molecules^{19,23} can be employed to predict spin-orbit branching fractions as a function of initial relative orientation of the collision partners, from both calculated and experimentally measured quantities. We use the NO + Ar collision system as an illustrative example, but the method could potentially be extended to larger systems, for which the identification of the optimum collision geometry that maximizes the yield of a certain product channel might be very valuable.

Owing to its unpaired electron, the NO molecule possesses a spin component and an electronic angular momentum with projections $\Sigma = \pm \frac{1}{2}$ and $\Lambda = \pm 1$, respectively, onto the intermolecular axis. This gives rise to two spin-orbit manifolds, specified by the spin-orbit quantum number $\Omega = \Sigma + \Lambda$. The lower lying state corresponds to $|\Omega| = \frac{1}{2}$ and the higher lying state to $|\Omega| = \frac{3}{2}$. Within both manifolds, each rotational state is further split into two Λ -doublet levels with symmetry indices 1 (e) and -1 (f). In our experiments, we employ a hexapole to select the initial $|j = \frac{1}{2}, m, |\Omega| = \frac{1}{2}, f\rangle$ quantum state of the NO molecules (where $j = \frac{1}{2}$ is the rotational ground state, which can only be oriented, and m its projection onto the relative velocity vector, \mathbf{k}), before subjecting them to a static electric field. In the electric field, the initially pure f state wave function evolves into a superposition of the e and f state wave functions, and their relative contributions, which are dependent on the strength of the electric field, are quantified by the mixing parameters α and β (see Supplementary Information).^{13,25} Since the f Λ -doublet state is low-field seeking, the dipole moment ($N \rightarrow O$) of the state selected molecules will orient antiparallel to the electric field vector, \mathbf{E} , due to the Stark effect. By switching the polarization of the electric field, we can change the orientation of the molecules in a given configuration by 180° .

We define the orientation of the electric field within the scattering frame, as illustrated in Figure 1. For the analysis presented below, we focus on in-plane (and near-side) scattering, with \mathbf{E} lying within the plane of the initial and final relative velocity vectors, \mathbf{k} and \mathbf{k}' , respectively. We can thus cover the full range of possible orientations by sampling the polar angle θ_E between $0^\circ - 180^\circ$ at fixed azimuthal angles of $\phi_E = 0^\circ$ and $\phi_E = 180^\circ$. Figures 1b and c also show the electric field vector and the most probable orientation of the NO molecule for the two side-on (b) and the two end-on (c) configurations. The labels “ $+x$ ” and “ $-x$ ” correspond to repulsive collisions of the Ar atom off the N-side and O-side, while “ $+z$ ” and “ $-z$ ” correspond to repulsive collisions towards the O-end and N-end, respectively (the labels indicate the direction of \mathbf{E} in each case).

As shown in our previous work,^{19,23} for an arbitrary orientation, defined by the electric field vector in the scattering frame, the differential cross section (DCS), for initial $j = \frac{1}{2}$, can be ex-

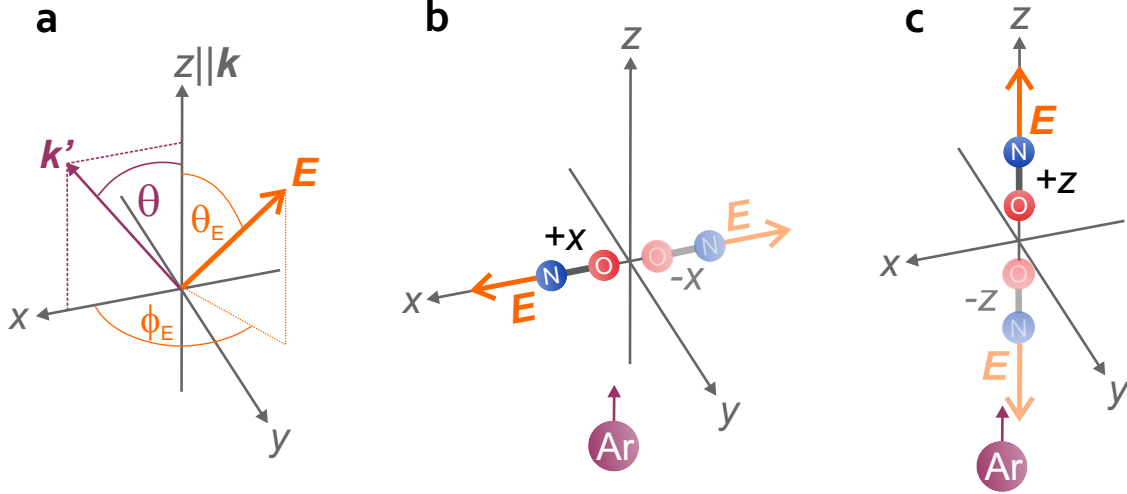


Figure 1: Definition of the electric field direction in the scattering frame (a), side-on orientation (b), and end-on orientation (c). The z -axis in the scattering frame is defined parallel to the relative velocity vector, $k = v_{\text{Ar}} - v_{\text{NO}}$, and the $+xz$ -plane is that containing k and k' , where $k' = v'_{\text{Ar}} - v'_{\text{NO}}$ is the relative velocity vector after the collision. θ is the scattering angle, and θ_E and ϕ_E are the polar and azimuthal angles of the electric field vector, E . The orientations of the NO molecule in (b) and (c) are labelled according to the axis along which E is pointing. **Note that the electric field creates a cosine distribution of possible NO orientations; the dipole moment pointing antiparallel to the E vector is the most probable one.**¹⁵

pressed in terms of the bond-axis polarization dependent differential cross sections (r -PDDCSs):^{19,26}

$$[d\sigma(\theta)]_{\theta_E}^{\phi_E} = \frac{\sigma_{\text{iso}}}{2\pi} \left[R_0^{(0)}(\theta) - |\alpha\beta| \left(\cos \theta_E R_0^{(1)}(\theta) - \sqrt{2} \sin \theta_E \cos \phi_E R_1^{(1)}(\theta) \right) \right]. \quad (1)$$

Here, σ_{iso} is the “isotropic” integral cross section (ICS) in the presence of a field, the $R_q^{(k)}(\theta)$ are the **r -polarization dependent cross sections**,^{19,26} and α and β are the field-dependent mixing parameters mentioned above.^{13,25} **The $R_q^{(k)}(\theta)$ quantify the dependence of the collision outcome on the polarization of the bond-axis (as a function of scattering angle), with the isotropic $R_0^{(0)}(\theta)$ moment equal to the normalized DCS in the absence of reagent polarization, but in the presence of an orientation field.**¹⁹

For a given θ_E angle, and $\phi_E = 0^\circ$ or $\phi_E = 180^\circ$, we can write,

$$[d\sigma(\theta)]_{\theta_E}^{\phi_E=0^\circ/180^\circ} = \frac{\sigma_{\text{iso}}}{2\pi} \left[R_0^{(0)}(\theta) - |\alpha\beta| \left(\cos \theta_E R_0^{(1)}(\theta) \pm \sqrt{2} \sin \theta_E R_1^{(1)}(\theta) \right) \right], \quad (2)$$

Computationally, the $R_q^{(k)}(\theta)$ moments can be calculated readily from the scattering amplitudes (see Supplementary Information). Experimentally, the $R_0^{(0)}(\theta)$ moment can be extracted from the sum of the velocity-map ion images for the two side-on, or the two end-on, orientations. Similarly, the $R_0^{(1)}(\theta)$ and $R_1^{(1)}(\theta)$ moments can be determined from the difference image for the two end-on and the two side-on orientations, respectively.^{19,23} Knowledge of all three $R_q^{(k)}(\theta)$ moments, and substitution into eq (1), would then allow calculation of the DCS at any arbitrary orientation. Note that for end-on orientation, $\theta_E = 0^\circ$ or 180° and the third term in eq (1) goes to zero, while for side-on orientation, $\theta_E = 90^\circ$, and the second term, containing the $R_0^{(1)}(\theta)$ moment, goes to zero.

To illustrate the above discussion, the $R_0^{(0)}(\theta)$ and $R_1^{(1)}(\theta)$ moments extracted from the ion images in the side-on orientation are compared to the QM calculated moments in Figure 2 for the $j' = 5.5e - 10.5e$ final states. Transitions within the ground spin-orbit manifold ($\Delta\Omega = 0$) are shown on the left-hand side, and transitions into the spin-orbit changing manifold ($\Delta\Omega = 1$) are shown on the right-hand side. The agreement between the experiment and calculations is good overall. The most significant deviations are observed in the $R_0^{(0)}(\theta)$ moment for $j' = 7.5e$ and $9.5e$ (in both spin-orbit manifolds), where the experimental moment is not quite able to reproduce the double-peaked features in the QM calculation. **This is because the main scattering intensity overlaps with the position of zero laboratory velocity, where even small inaccuracies in the instrument function become magnified.**²³

The spin-orbit branching fraction, that is, the fraction of the spin-orbit changing transition to the sum of the transitions into both manifolds, can then be evaluated at any given orientation:

$$\left[d\sigma_{\text{frac}} \right]_{\theta_E}^{\phi_E=0^\circ/180^\circ} = \frac{\left[d\sigma_{\Delta\Omega=1} \right]_{\theta_E}^{\phi_E=0^\circ/180^\circ}}{\left[d\sigma_{\Delta\Omega=1} \right]_{\theta_E}^{\phi_E=0^\circ/180^\circ} + \left[d\sigma_{\Delta\Omega=0} \right]_{\theta_E}^{\phi_E=0^\circ/180^\circ}} . \quad (3)$$

The ability to determine the differential branching fraction at any arbitrary orientation enables us to quantify the extent of control over the collision outcome achievable by varying the collision geometry. Figure 3 shows the QM calculated branching fractions as a function of the scattering angle, θ (y-axis), and the initial relative orientation of the NO and Ar collision partners, **as defined**

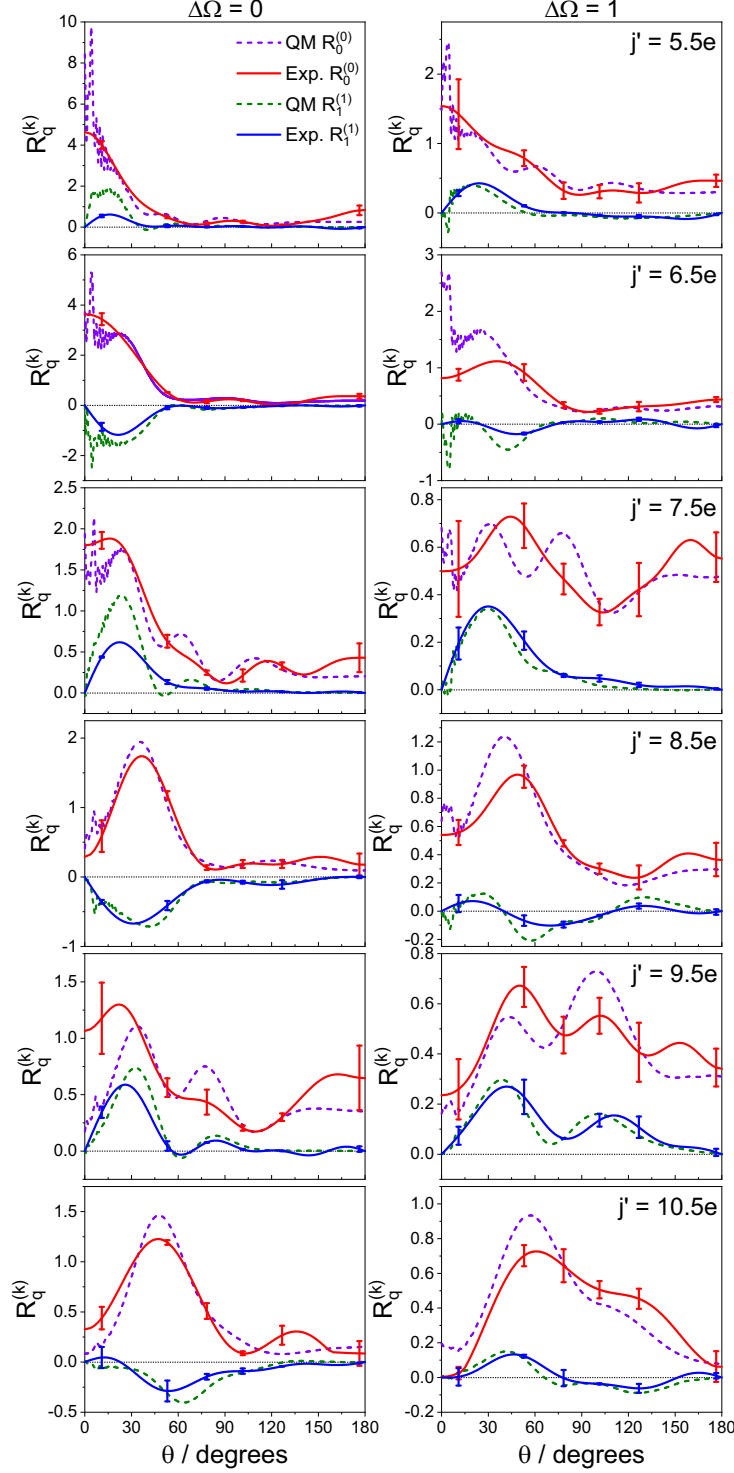


Figure 2: Comparison of the experimental and QM calculated polarization moments for $j' = 5.5e - 10.5e$ (top to bottom) in the spin-orbit conserving ($\Delta\Omega = 0$, left, taken from ref 23) and changing ($\Delta\Omega = 1$, right) manifolds. The experimental $R_0^{(0)}(\theta)$ and $R_1^{(1)}(\theta)$ moments are shown in red and blue, and their QM counterparts are represented by the purple and green dashed lines, respectively. The error bars in the experimental data correspond to one standard deviation. The QM data were averaged over the experimental collision energy distribution with a mean of 651 cm^{-1} .

by the angles of the electric field, θ_E and ϕ_E (x -axis in the figure). The branching fractions are shown for $j' = 5.5e - 10.5e$; the right panel for each state corresponds to $\phi_E = 0^\circ$ and the left panel to $\phi_E = 180^\circ$. Note that $\theta_E = 0^\circ$ corresponds to the $+z$ (O-end) orientation and $\theta_E = 180^\circ$ to the $-z$ (N-end) orientation, irrespective of ϕ_E . The $\pm z$ and $\pm x$ orientations are indicated at the top of the figure. Red indicates dominance of the spin-orbit changing transition ($d\sigma_{\text{frac}} > 0.5$), while yellow indicates dominance of the spin-orbit conserving transition ($d\sigma_{\text{frac}} < 0.5$). The maxima in the spin-orbit fractions are due to some combination of local maximum, or significant scattering intensity, in the spin-orbit changing manifold, and local minimum, or low scattering intensity, in the spin-orbit conserving manifold.

It is remarkable how the spin-orbit branching fraction can be changed by varying the orientation of the electric field. Figure 3 demonstrates that, if the initial geometry of the collision system can be defined, the relative yields of specific product channels at a given scattering angle can be controlled. For example, in the case of $j' = 8.5e$ the contribution of $\Omega' = \frac{3}{2}$ can be maximized to $d\sigma_{\text{frac}} \approx 1$ in the backward scattered region by setting the orientation field nearly perpendicular to the relative velocity vector ($-z$ orientation). Conversely, its contribution at the same scattering angles can be reduced to less than 0.1 by setting $\theta_E = 45^\circ$ and $\phi_E = 180^\circ$. Analogously, if we wanted to optimize the relative yield of spin-orbit changing products in the backward scattered region of the $j' = 6.5e$ state, we would orient the electric field in our experiment at the angles of $\theta_E \sim 135^\circ$ and $\phi_E = 0^\circ$. A similar dependence of the branching fraction on the initial orientation is observed for the other j' states shown in Figure 3. This dependence can be interpreted in a general picture in which reactants follow a certain pathway to products depending on their initial position on the potential energy surface (PES) and the internal and translational energy they possess at that point. By carefully choosing the initial geometry, a scattering process or reaction can thus be tuned in favor of a particular outcome.

By integration of the differential cross sections for given θ_E and ϕ_E angles, we can test whether the dependence on the initial relative orientation survives in the integral spin-orbit branching frac-

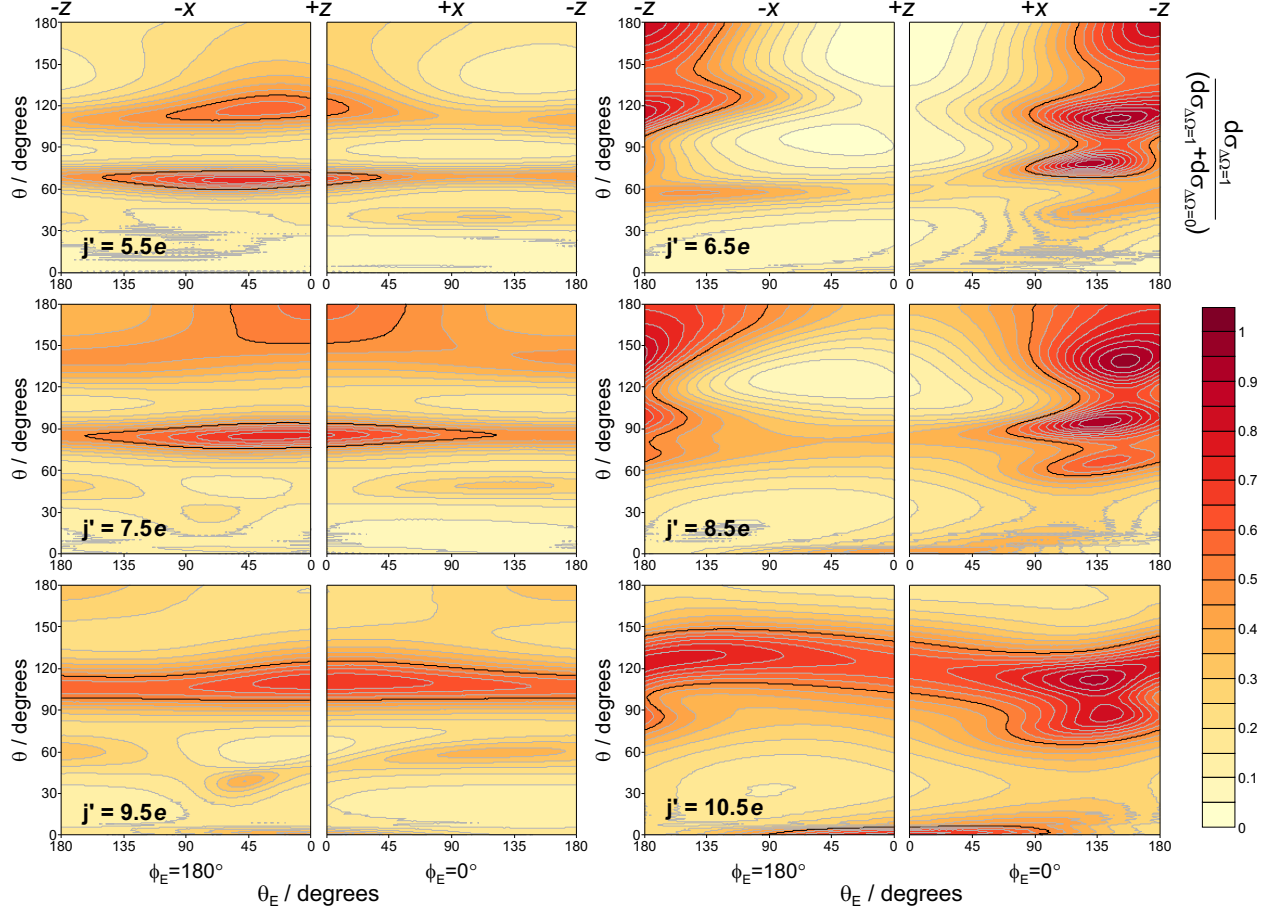


Figure 3: Contour plots showing the differential QM spin-orbit branching fractions as a function of the scattering angle, θ (y-axis), and the polar angle of the electric field, θ_E (x-axis), for $j' = 5.5e - 10.5e$. The θ_E angles corresponding to the $\pm z$ and the $\pm x$ configurations are indicated at the top. Note that the right-hand side for each state corresponds to $\phi_E = 0^\circ$ and the left-hand side to $\phi_E = 180^\circ$. The black contour indicates a branching fraction of 0.5. The calculations were run at the experimental field strength using a collision energy of 651 cm^{-1} .

tions. The integral cross sections are obtained by integrating the DCSs in eq (2):

$$\sigma_{\theta_E}^{\phi_E=0^\circ/180^\circ} = \frac{\sigma_{\text{iso}}}{2\pi} \left[r_0^{(0)} - |\alpha\beta| \left(\cos \theta_E r_0^{(1)} \pm \sqrt{2} \sin \theta_E r_1^{(1)} \right) \right], \quad (4)$$

where the $r_q^{(k)}$ moments are the integrated $R_q^{(k)}(\theta)$ moments,²⁶

$$r_q^{(k)} = \int_{-1}^{+1} R_q^{(k)}(\theta) d(\cos \theta). \quad (5)$$

Since $R_0^{(0)}$ is the normalized isotropic DCS, $r_0^{(0)}$ is equal to one. The $r_1^{(1)}$ and $r_0^{(1)}$ moments, for their part, are directly related to the integral steric asymmetry (ISA) for the x - and z -axis orientations, respectively,²³

$$r_1^{(1)} = \frac{S_x}{\sqrt{2}|\alpha\beta|}, \quad (6)$$

$$r_0^{(1)} = \frac{S_z}{|\alpha\beta|}, \quad (7)$$

where S_x and S_z are the ISAs for the x -axis (side-on) and z -axis (end-on) configurations, respectively, as defined in the Supplementary Information. The ISA is a measure of the integral preference of one orientation over the other for a given product rotational state. Using the relationships in eq (6) and (7), the integral cross sections can be rewritten in terms of S_x and S_z :

$$\sigma_{\theta_E}^{\phi_E=0^\circ/180^\circ} = \frac{\sigma_{\text{iso}}}{2\pi} (1 - \cos \theta_E S_z \pm \sin \theta_E S_x). \quad (8)$$

The integral cross sections can thus be calculated solely from the experimental (or QM) ISAs in the side-on and the end-on orientations. Using the integral cross sections for both spin-orbit manifolds, the integral spin-orbit branching fractions can be calculated analogously to the differential branching fractions:

$$\left[\sigma_{\text{frac}} \right]_{\theta_E}^{\phi_E=0^\circ/180^\circ} = \frac{\left[\sigma_{\Delta\Omega=1} \right]_{\theta_E}^{\phi_E=0^\circ/180^\circ}}{\left[\sigma_{\Delta\Omega=1} \right]_{\theta_E}^{\phi_E=0^\circ/180^\circ} + \left[\sigma_{\Delta\Omega=0} \right]_{\theta_E}^{\phi_E=0^\circ/180^\circ}}. \quad (9)$$

The top panel in Figure 4 shows the experimental integral branching fractions obtained using the S_x and S_z values from previous measurements.^{15,21,23,24} These are compared with the QM calculated branching fractions in the bottom panel. Since in these experiments we have not measured the relative cross sections for the two spin-orbit manifolds, proportional to σ_{iso} , the experimental ICS ratios were scaled to the QM ICS ratios to allow a direct comparison between experiment and theory. The theoretical isotropic spin-orbit branching fractions and their dependence on the static field strength are shown in the Supplementary Information. Note that, in principle, the required cross section ratios for spin-orbit conserving and changing collisions could be determined relatively straightforwardly from the resonantly enhanced multiphoton ionization (REMPI) spectrum or laser induced fluorescence measurements of the scattered NO(X), as has been undertaken in previous work.^{27,28}

The experimental and QM field-dependent integral spin-orbit branching fractions shown in Figure 4 are in good agreement, which is not unexpected given the generally excellent agreement between experimental and QM integral steric asymmetries found in the previous studies.^{15,21,23,24} As already observed in the differential branching fractions (Figure 3), the integral branching fractions vary as a function of electric field orientation, roughly averaging between 0.2 - 0.3. The variations are more pronounced for the even Δj transitions (purple lines), where the fractions span a range from about 0.1 to 0.45, and are more subtle for the odd Δj transitions (orange lines). Comparison with Figure 3 reveals that the maxima for the even Δj transitions around $\theta_E = 135^\circ / \phi_E = 0^\circ$ are mainly due to a strong spin-orbit excited contribution in the backward scattered region ($\theta \geq 60^\circ$).

The integral steric asymmetries measured in the side-on and the end-on orientations exhibited an N-side/N-end preference for odd Δj , and an O-side/O-end preference for even Δj in both spin-orbit manifolds.^{15,21,23,24} However, while the magnitude of the N-side/N-end preference was relatively similar in the two manifolds, the magnitude for O-side/O-end collisions was significantly diminished, and an overall preference for N-side/N-end collisions was observed, in the spin-orbit excited state.^{21,24} Alexander has shown²⁹ that for pure Hund's case (a) molecules, $\Delta\Omega = 0$ and $\Delta\Omega = 1$ transitions can be assumed to occur on the half-sum (V_{sum}) and half-difference (V_{diff}) po-

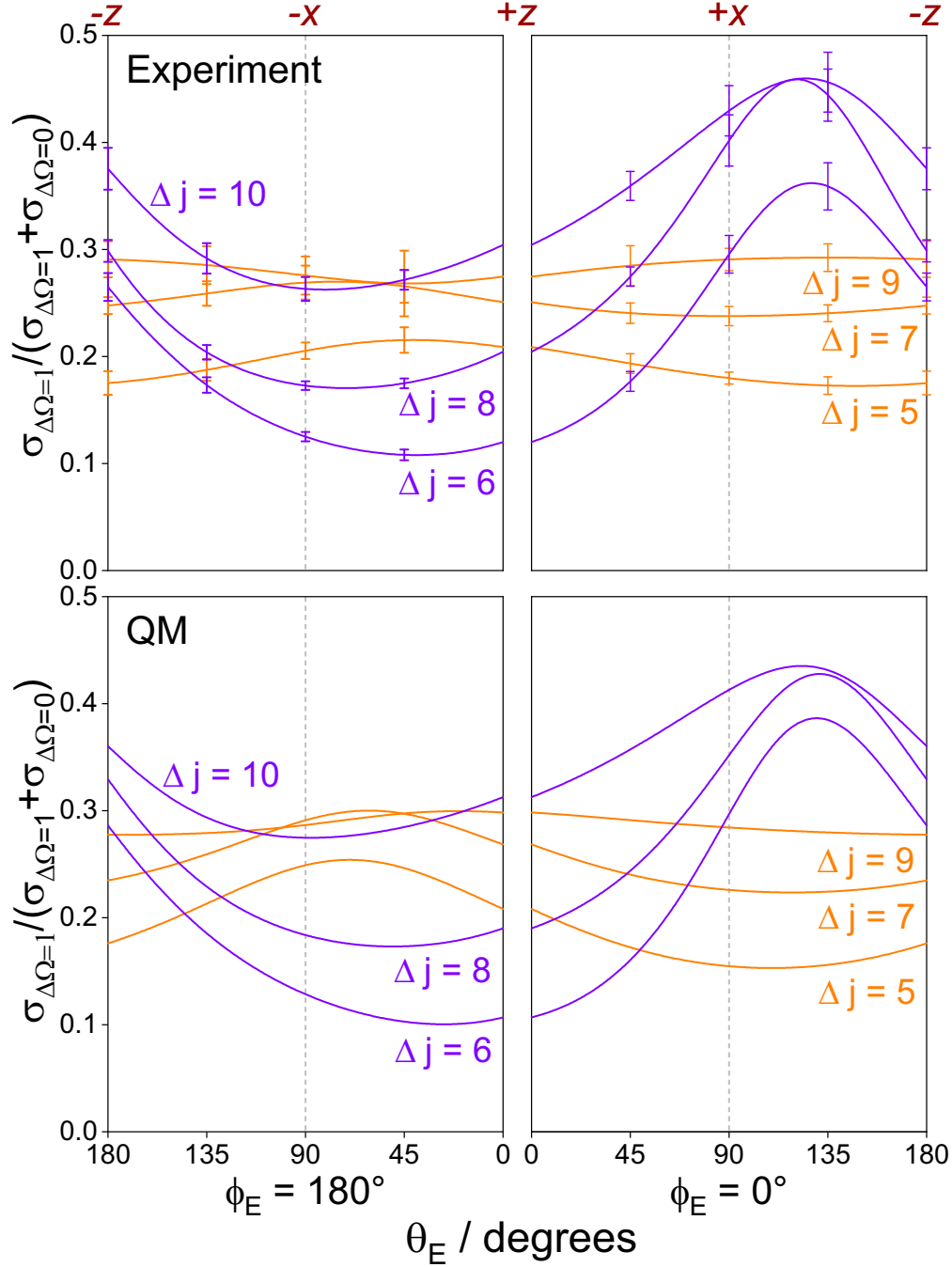


Figure 4: Fraction of the spin-orbit changing integral cross section to the sum of the ICSs for the two spin-orbit manifolds, as a function of θ_E , for $j' = 5.5e - 10.5e$. The top panel shows the fractions obtained from the experimental steric asymmetries (with error bars representing one standard deviation); the bottom panel shows the calculated QM fractions, which have been averaged over the experimental collision energy distribution. Even Δj transitions are represented in purple, and odd Δj transitions in orange. The θ_E angles corresponding to the $\pm z$ and the $\pm x$ configurations are indicated at the top of the figure. The right-hand side corresponds to $\phi_E = 0^\circ$ and the left-hand side to $\phi_E = 180^\circ$.

tentials, respectively. These potentials reflect the preferential location of the unpaired electron lying closer to the N atom of the NO molecule, either in or out of the plane defined by the three atoms (corresponding to the A' and A'' PESs, respectively^{29–31}). The configuration in which the electron is in the plane of the three atoms (i.e. on the A' PES) facilitates the interaction between the incoming Ar atom and the lone electron necessary for spin-orbit changing transitions to occur.²⁴ The maxima for the even Δj transitions around $\theta_E = 135^\circ/\phi_E = 0^\circ$ in Figure 4, which correspond to collisions near the N atom, are a manifestation of the overall shift towards an N-side/N-end preference. The opposite orientation, corresponding to $\theta_E \sim 45^\circ/\phi_E = 180^\circ$, is in the region of the minima of the branching fractions. Thus, placing the electric field at approximately $\theta_E = 135^\circ$ from the relative velocity vector will maximize the spin-orbit changing integral fraction for the even Δj transitions, when the Ar atom approaches towards the N atom, while concomitantly minimizing the fraction for trajectories towards the O atom.

Our analysis of the spin-orbit branching fractions shows that the ability to select the initial orientation of the NO molecules prior to collision provides a large degree of control over the spin-orbit branching fraction. The implications of our results may be generalized to other systems with an asymmetric PES and at least two competing product channels. We expect that the more asymmetric the potential energy landscape, the more important the initial orientation will be in defining the relative populations of the accessible product states. In the current work, the maxima of the spin-orbit changing fractions for the even Δj transitions near the N atom of the molecule reflect the position of the unpaired electron,²⁴ and it might be expected that other collision processes or reactions, in which unpaired or weakly bound electrons are involved, will show a similar sensitivity to the location of the relevant electronic orbitals. The current QM treatment can be applied to other linear open-shell molecules, such as OH, which is slightly more complex than NO due to its $|\Omega| = \frac{3}{2}$ ground spin-orbit state. Although the degree of complexity will increase further, we believe that it is also possible to extend the theory to symmetric and asymmetric tops. The capabilities of the experimental methods used in our study could be expanded as well. In particular, it might be possible to perform laser alignment within an electric field³² so that “heads” and “tails” may

be distinguished. This would provide a means for state selection without the need of a hexapole and the limitation to energetically low-lying quantum states. Moreover, it will be interesting to see if full control over the initial geometry can be implemented in collision processes and reactions in solution, on surfaces, or on gas-liquid interfaces.

Acknowledgments

F.J.A. and P.G.J. thank Prof. Enrique Verdasco for his help with the calculations. Funding by the UK EPSRC (to M.B. *via* Programme Grant EP/L005913/1 and EP/T021675/1) and the Spanish Ministry of Science and Innovation (grant MINECO/FEDER-PGC2018-096444-B-I00) is gratefully acknowledged. P.G.J. acknowledges funding by the Fundación Salamanca City of Culture and Knowledge (programme for attracting scientific talent to Salamanca).

Supporting Information

Computational and experimental methods, **branching fractions for an isotropic distribution in the presence and absence of an electric field.**

References

- (1) Pan, H.; Wang, F.; Czakó, G.; Liu, K. Direct mapping of the angle-dependent barrier to reaction for $\text{Cl} + \text{CHD}_3$ using polarized scattering data. *Nat. Chem.* **2017**, *9*, 1175–1180.
- (2) Sun, Z.-F.; van Hemert, M. C.; Loreau, J.; van der Avoird, A.; Suits, A. G.; Parker, D. H. Molecular square dancing in CO-CO collisions. *Science* **2020**, *369*, 307–309.
- (3) de Miranda, M. H. G.; Chotia, A.; Neyenhuis, B.; Wang, D.; Quémener, G.; Ospelkaus, S.; Bohn, J. L.; Ye, J.; Jin, D. S. Controlling the quantum stereodynamics of ultracold bimolecular reactions. *Nat. Phys.* **2011**, *7*, 502–507.
- (4) Xie, Y.; Zhao, H.; Wang, Y.; Huang, Y.; Wang, T.; Xu, X.; Xiao, C.; Sun, Z.; Zhang, D. H.; Yang, X. Quantum interference in $\text{H} + \text{HD} \rightarrow \text{H}_2 + \text{D}$ between direct abstraction and roaming insertion pathways. *Science* **2020**, *368*, 767–771.
- (5) Loesch, H. J.; Remscheid, A. Brute force in molecular reaction dynamics: A novel technique for measuring steric effects. *J. Chem. Phys.* **1990**, *93*, 4779–4790.
- (6) Gijsbertsen, A.; Linnartz, H.; Taatjes, C. A.; Stolte, S. Quantum interference as the source of steric asymmetry and parity propensity rules in NO-rare gas inelastic scattering. *J. Am. Chem. Soc.* **2006**, *128*, 8777–8789.
- (7) Perreault, W. E.; Mukherjee, N.; Zare, R. N. Quantum control of molecular collisions at 1 kelvin. *Science* **2017**, *358*, 356–359.
- (8) Perreault, W. E.; Mukherjee, N.; Zare, R. N. HD ($v = 1, j = 2, m$) orientation controls HD–He rotationally inelastic scattering near 1 K. *J. Chem. Phys.* **2019**, *150*, 174301.
- (9) Wang, F.; Lin, J.; Liu, K. Steric control of the reaction of CH stretch–excited CHD_3 with chlorine atom. *Science* **2011**, *331*, 900–903.

- (10) Perreault, W. E.; Mukherjee, N.; Zare, R. N. Cold quantum-controlled rotationally inelastic scattering of HD with H₂ and D₂ reveals collisional partner reorientation. *Nat. Chem.* **2018**, *10*, 561–567.
- (11) Sharples, T. R.; Leng, J. G.; Luxford, T. F. M.; McKendrick, K. G.; Jambrina, P. G.; Aoiz, F. J.; Chandler, D. W.; Costen, M. L. Non-intuitive rotational reorientation in collisions of NO(A²Σ⁺) with Ne from direct measurement of a four-vector correlation. *Nat. Chem.* **2018**, *10*, 1148–1153.
- (12) Jones, E. M.; Brooks, P. R. Focusing and orienting asymmetric-top molecules in molecular beams. *J. Chem. Phys.* **1970**, *53*, 55–58.
- (13) van Leuken, J.; Bulthuis, J.; Stolte, S.; Snijders, J. Steric asymmetry in rotationally inelastic state-resolved NO-Ar collisions. *Chem. Phys. Lett.* **1996**, *260*, 595–603.
- (14) van Beek, M. C.; Berden, G.; Bethlem, H. L.; ter Meulen, J. J. Molecular reorientation in collisions of OH+Ar. *Phys. Rev. Lett.* **2001**, *86*, 4001–4004.
- (15) Nichols, B.; Chadwick, H.; Gordon, S. D. S.; Eyles, C. J.; Hornung, B.; Brouard, M.; Alexander, M. H.; Aoiz, F. J.; Gijsbertsen, A.; Stolte, S. Steric effects and quantum interference in the inelastic scattering of NO(X) + Ar. *Chem. Sci.* **2015**, *6*, 2202–2210.
- (16) Boca, A.; Friedrich, B. Fine structure, alignment, and orientation of ³²S¹⁶O and ¹⁶O¹⁸O molecules in congruent electric and magnetic fields. *J. Chem. Phys.* **2000**, *112*, 3609–3619.
- (17) Zou, J.; Gordon, S. D. S.; Tanteri, S.; Osterwalder, A. Stereodynamics of Ne(³P₂) reacting with Ar, Kr, Xe, and N₂. *J. Chem. Phys.* **2018**, *148*, 164310.
- (18) Gordon, S. D. S.; Omiste, J. J.; Zou, J.; Tanteri, S.; Brumer, P.; Osterwalder, A. Quantum-state-controlled channel branching in cold Ne(³P₂) + Ar chemi-ionization. *Nat. Chem.* **2018**, *10*, 1190–1195.

- (19) Heid, C. G.; Walpole, V.; Brouard, M.; Aoiz, F. J.; Jambrina, P. G. Side-impact collisions of Ar with NO. *Nat. Chem.* **2019**, *11*, 662–668.
- (20) Brouard, M.; Chadwick, H.; Gordon, S. D. S.; Hornung, B.; Nichols, B.; Aoiz, F. J.; Stolte, S. Stereodynamics in NO(X) + Ar inelastic collisions. *J. Chem. Phys.* **2016**, *144*, 224301.
- (21) Brouard, M.; Gordon, S. D. S.; Hackett Boyle, A.; Heid, C. G.; Nichols, B.; Walpole, V.; Aoiz, F. J.; Stolte, S. Integral steric asymmetry in the inelastic scattering of NO(X²Π). *J. Chem. Phys.* **2017**, *146*, 014302.
- (22) Brouard, M.; Gordon, S. D. S.; Nichols, B.; Walpole, V.; Aoiz, F. J.; Stolte, S. Differential steric effects in the inelastic scattering of NO(X) + Ar: Spin–orbit changing transitions. *Phys. Chem. Chem. Phys.* **2019**, *21*, 14173–14185.
- (23) Walpole, V.; Heid, C. G.; Jambrina, P. G.; Aoiz, F. J.; Brouard, M. Steric effects in the inelastic scattering of NO(X) + Ar: Side-on orientation. *J. Phys. Chem. A* **2019**, *123*, 8787–8806.
- (24) Heid, C. G.; Benthams, I. P.; Walpole, V.; Gheorghe, R.; Jambrina, P. G.; Aoiz, F. J.; Brouard, M. Probing the location of the unpaired electron in spin-orbit changing collisions of NO with Ar. *Phys. Chem. Chem. Phys.* **2020**, *22*, 22289–22301.
- (25) de Lange, M.; Drabbels, M.; Griffiths, P.; Bulthuis, J.; Stolte, S.; Snijders, J. Steric asymmetry in state-resolved NO–Ar collisions. *Chem. Phys. Lett.* **1999**, *313*, 491–498.
- (26) Aoiz, F. J.; Martínez, M. T.; Sáez Rábanos, V. Quasi-classical treatment of the stereodynamics of chemical reactions: $\mathbf{k-r-k'}$ vector correlation for the Li + HF($v = 1, j = 1$) → LiF + H reaction. *J. Chem. Phys.* **2001**, *114*, 8880–8896.
- (27) Lin, A.; Antonova, S.; Tsakotellis, A. P.; McBane, G. C. A Doublet propensities in Ar-NO rotationally inelastic scattering at 220 meV. *J. Phys. Chem. A* **1999**, *103*, 1198–1205.

- (28) Joswig, H.; Andresen, P.; Schinke, R. Electronic fine structure transitions and rotational excitation in NO rare gas collisions. *J. Chem. Phys.* **1986**, *85*, 1904–1914.
- (29) Alexander, M. H. Rotationally inelastic collisions between a diatomic molecule in a $^2\Pi$ electronic state and a structureless target. *J. Chem. Phys.* **1982**, *76*, 5974–5988.
- (30) Alexander, M. H. Quantum treatment of rotationally inelastic collisions involving molecules in Π electronic states: New derivation of the coupling potential. *Chem. Phys.* **1985**, *92*, 337–344.
- (31) Alexander, M. H. Differential and integral cross sections for the inelastic scattering of NO($X^2\Pi$) by Ar based on a new *ab initio* potential energy surface. *J. Chem. Phys.* **1993**, *99*, 7725–7738.
- (32) Friedrich, B.; Herschbach, D. Manipulating molecules via combined static and laser fields. *J. Phys. Chem. A* **1999**, *103*, 10280–10288.